PHYSICAL REVIEW B **82**, 024421 (2010)

Magnetization distribution in the tetragonal phase of $BaFe_2As_2$

P. J. Brown,[1,2] T. Chatterji,[3] A. Stunault,[1] Y. Su,[4] Y. Xiao,[5] R. Mittal,[4,6] Th. Brückel,[4,5] Th. Wolf,[7] and P. Adelmann[7]
[1]*Institut Laue-Langevin, BP 156, 38042 Grenoble Cedex 9, France*
[2]*Department of Physics, Loughborough University, Loughborough LE11 3TU, United Kingdom*
[3]*JCNS, Forschungszentrum Jülich, Outstation at Institut Laue-Langevin, BP 156, 38042 Grenoble Cedex 9, France*
[4]*JCNS, Forschungszentrum Jülich, Outstation at FRM II, Lichtenbergstrasse 1, 85747 Garching, Germany*
[5]*Institut für Feskörperforschung, Forschungszentrum Jülich, 52425 Jülich, Germany*
[6]*Solid State Physics Division, Bhabha Atomic Research Centre, Trombay, Mumbai 400085, India*
[7]*Karlsruhe Institute of Technology, Institut fuer Festkoerperphysik, D-76021 Karlsruhe, Germany*
(Received 4 June 2010; revised manuscript received 6 July 2010; published 21 July 2010)

We have determined the spatial distribution of the magnetization induced by a field of 9 T in the tetragonal phase of $BaFe_2As_2$ using polarized neutron diffraction. Magnetic structure factors derived from the polarization dependence of the intensities of Bragg reflections were used to make a maximum-entropy reconstruction of the distribution projected on the 110 plane. The reconstruction shows clearly that the magnetization is confined to the region around the iron atoms and that there is no significant magnetization associated with either As or Ba atoms. The distribution of magnetization around the Fe atom is significantly nonspherical with a shape which is extended in the $\langle 111 \rangle$ directions in the projection. These results show that the electrons which give rise to the paramagnetic susceptibility are confined to the Fe atoms their distribution suggests that they occupy $3d$ t_{2g}-type orbitals with $\approx 60\%$ in those of xy symmetry.

DOI: 10.1103/PhysRevB.82.024421 PACS number(s): 75.25.−j

The pnictide superconductors and their parent compounds have drawn extensive attention because they provide a new opportunity to investigate the mechanism of non-BCS exotic superconductivity.[1–5] Most of the research on pnictide superconductors has focused on two classes of compounds, RFeAs(O_xF_{1-x}) (with R=La, Nd, and Sm) and $A$$Fe_2As_2$ (with A=Ba, Ca, and Sr), the so called "1111" and "122" families. Both these two classes of compounds adopt a layered structure with a single FeAs layer in the unit cell of 1111 and two such layers in the unit cell of "122." The superconducting state can be induced either by electron or hole doping of the parent compounds or also by pressure.[6–8] Till now, the highest T_c attained is 57.4 K in the electron-doped $Ca_{0.4}Na_{0.6}FeAsF$ 1111 compound[9] while for 122 family the highest T_c of 38 K is reached in the hole-doped $Ba_{0.6}K_{0.4}Fe_2As_2$.[5] The 122 compounds differ from the cuprate superconductors in that the superconducting state can be induced by the application of pressure only.[10,11] It seems that the FeAs layers are responsible for superconductivity in these compounds because the electronic states near the Fermi surface are dominated by contributions from Fe and As. Recent neutron-diffraction experiments reveal that the common feature of all the iron pnictide parent compounds[12–16] is a spin-density wave arising from long-range antiferromagnetic (AFM) order of the Fe moments at low temperature. For the parent compounds the onset of AFM order coincides with the tetragonal-orthorhombic structural phase transition in the 122 family and is preceded by it in the 1111 family. The role of orbital ordering in driving these transitions and leading to anisotropic magnetic coupling is still being debated.[17] Phase diagrams of some iron pnictides show clearly that the magnetic order can be suppressed by charge-carrier doping of the parent compound. Concomitantly, superconductivity emerges and reaches a maximum T_c at optimal doping,[18] thus exhibiting features similar to high-T_c cuprates.[19] Extensive studies of phonon dynamics[20,21] suggest that it is unlikely that the superconductivity in iron pnictides is due to simple electron-phonon coupling. Since it seems that phonons play no significant role in the superconducting pair formation, it is natural to presume that magnetism has a crucial role in the appearance of superconductivity and consequently AFM spin fluctuations have been suggested as a possible pairing mechanism. Strong evidence for the presence of resonant spin excitations in the superconducting phase has indeed been obtained from recent inelastic neutron-scattering experiments on several optimally doped 122 superconductors.[22–24]

The nature of magnetism and possible orbital order in iron pnictide compounds are still very controversial and therefore additional experimental information on these degrees of freedom for the parent compounds can be helpful in understanding the nature of superconductivity in these compounds. In order to get direct information about the electronic structure of the parent 122 compound we have undertaken a polarized neutron-diffraction experiment on $BaFe_2As_2$ to determine the field-induced magnetization distribution. A good quality single crystal was grown by the self-flux method. The structural parameters were determined from unpolarized neutron integrated intensity measurements made using the four-circle diffractometer D9 and flipping ratios were measured using the polarized neutron diffractometer D3. Both these instruments are installed on the hot neutron source of the high-flux reactor of the Institute Laue-Langevin in Grenoble. The sample was held at constant temperature in a closed-cycle refrigerator on D9 whereas on D3 it was oriented with a $\langle 1\bar{1}0 \rangle$ axis parallel to the vertical field direction of a 9 T cryomagnet. The flipping ratios from the crystal were measured in the paramagnetic tetragonal phase at T=200 K.

Sets of experimental structure factors containing 70 independent reflections $\sin\theta/\lambda < 0.85$ Å^{-1} measured with λ =0.84 Å and 90 with $\sin\theta/\lambda < 1.0$ Å^{-1} and λ=0.52 Å

TABLE I. Parameters obtained in least-squares refinements of integrated intensities measured at $T=200$ K on D9.

Atom	Position in $I4/mcm$				z	B (Å^2)
Ba	2a	0	0	0		0.62(4)
Fe	4d	$\frac{1}{2}$	0	$\frac{1}{4}$		0.43(3)
As	4e	0	0	z	0.3543(1)	0.55(3)
Extinction			g (rad^{-1})		1.4(1.6)	
R_{cryst}	$\lambda=0.84$ Å		3.8		$\lambda=0.51$ Å	2.7

were obtained from the integrated intensities measured on D9 after averaging the intensities over equivalent reflections. These data were used in least-squares refinements of the crystal structure in which the variable parameters were the z coordinate of As, the isotropic temperature factors for the three sites and a single extinction parameter g representing the mosaic spread of the crystal. The results are summarized in Table I. The small value obtained for g, which is less than its estimated error, shows that any extinction is very small.

The ratios between the intensity scattered by the Bragg reflections in the $[1\bar{1}0]$ zone for incident neutrons polarized parallel and antiparallel to the applied field of 9 T (polarized neutron flipping ratios) were measured at 200 K using a neutron wavelength 0.825 Å. Since the susceptibility of $BaFe_2As_2$ is small $<2\times10^{-5}$ emu/g, all the flipping ratios R are close to unity and since the magnetic structure factors are proportional to $R-1$, it was necessary to record more than 10^7 neutrons from each reflection to obtain $\approx5\%$ precision. The flipping ratios measured for equivalent reflections and for repeated measurements of the same reflection were averaged together to give a mean value of R and used to calculate the magnetic structure factors F_M using the relationship

$$F_M = \frac{(R-1)F_N}{2(P^+ + P^-)},$$

where P^+ and P^- are the efficiencies of neutron polarization parallel and antiparallel to the applied field; F_N is the nuclear structure factor which was calculated using the parameters obtained from the integrated intensity measurements which are given in Table I.

TABLE II. Observed and calculated magnetic structure factors for the tetragonal phase of $BaFe_2As_2$ at 200 K.

h	k	l	$\sin\theta/\lambda$ (Å^{-1})	F_{dia} [a] (mμ_B)	F_{para} [b] (mμ_B)	F_{calc} [c] (mμ_B)	F_{calc} [d] (mμ_B)
0	0	2	0.077	0.48	−23.7(1.1)	−25.5	−24.4
0	0	4	0.154	−0.77	19.6(1.1)	21.3	20.9
1	1	2	0.195	−1.09	18.3(1.4)	18.6	17.5
1	1	4	0.236	0.59	−17(2)	−15.8	−15.4
1	1	6	0.292	−1.06	12.5(1.4)	12.2	12.5
0	0	8	0.308	−0.92	13(3)	11.3	11.9
2	2	0	0.357	−0.88	8.0(1.4)	8.7	8.1
2	2	2	0.366	0.25	−12(2)	−8.3	−7.9
0	0	10	0.386	0.41	−10(2)	−7.4	−8.1
2	2	4	0.389	−0.32	10(2)	7.3	7.3
1	1	10	0.425	−0.24	6(2)	5.9	6.7
0	0	12	0.463	−0.38	7(4)	4.6	5.2
2	2	8	0.472	−0.45	10(3)	4.4	5.3
1	1	12	0.496	0.10	−2(5)	−3.7	−4.5
2	2	10	0.526	0.23	−4(4)	−3.0	−4.1
3	3	2	0.542	−0.22	−2(5)	2.7	3.2

[a]Diamagnetic contribution to the magnetic structure factor.

[b]$F_{para}=F_M-F_{dia}$.

[c]Structure factors calculated with an Fe moment of 0.0068 μ_B and a spherically symmetric neutral Fe form factor (Ref. 28).

[d]Structure factors calculated using the multipole model with the parameters of the t_{2g} only model in Table III.

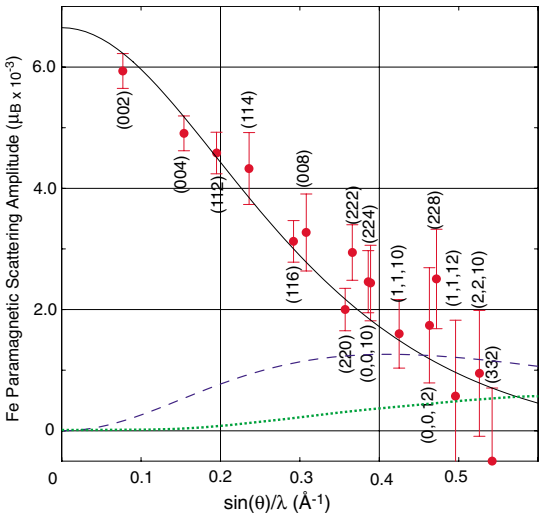

FIG. 1. (Color online) Paramagnetic scattering amplitudes measured for Fe in $BaFe_2As_2$ at 200 K. The solid curve shows the $\langle j_0 \rangle$ form factor for neutral Fe, Ref. 28, scaled to the paramagnetic magnetization of 6.65×10^{-3} μ_B/Fe. The dashed (blue) and the dotted (green) curves show $\langle j_2 \rangle$ and $\langle j_4 \rangle$ form factors, which multiply the anisotropic terms in the magnetic scattering on the same scale.

The magnetization induced in a crystal from the same batch as the one used in the experiment, by a field of 9 T applied the 001 plane at 200 K was measured as 0.0100 μ_B/f.u. It is the sum of a paramagnetic part due to magnetic excitation of electrons near the Fermi surface and a diamagnetic part to which all electrons contribute. The diamagnetic volume susceptibility is given by the Langevin equation.

$$\chi_{dia} = -(e^2/6Vmc^2)\sum_i Z_i \langle r^2 \rangle_i$$

the sum is over all the atoms i in the unit cell of volume V, $\langle r^2 \rangle_i$ is the mean-square radius of the ith atom's electron wave function, and Z_i its atomic number. The diamagnetic contribution to the magnetic structure factor is

$$F_{dia} = \frac{HC}{|\mathbf{k}|}\sum_i \frac{df(k)_i}{dk} \exp \imath \mathbf{k} \cdot \mathbf{r}_i, \qquad (1)$$

where $f_i(k)$ is the atomic form factor of the ith atom and $\mathbf{r}_i$ its position in the unit cell. The constant C has the value 1.52×10^{-5} $\mu_B T^{-1} Å^2$.[25,26] The diamagnetic contribution to the magnetization calculated using the atomic form factors for Ba, Fe, and As (Ref. 27) is −0.0033 μ_B/f.u., the paramagnetic part of the magnetization is therefore 0.0100−(−0.0033)=0.0133 μ_B/f.u.. The diamagnetic contributions to the magnetic structure factors were calculated using Eq. (1) and are given in Table II. The values F_{dia} were subtracted from the magnetic structure factors F_M obtained from the flipping ratios to give the paramagnetic structure factors F_{para} also listed in Table II.

An effective form factor for the Fe atom, obtained by dividing each F_{para} by the geometric structure factor of Fe for that reflection (4 for $h+k+l$ even and −4 for $h+k+l$ odd) is shown in Fig. 1 where it is compared with the Fe 3d free atom curve[28] scaled to 6.65 μ_B. The low-angle reflections fall on the curve within experimental error but at higher angles, at which the higher order form factors $\langle j_2 \rangle$ and $\langle j_4 \rangle$ become appreciable, significant scatter is apparent which may characterize an aspherical magnetization distribution.

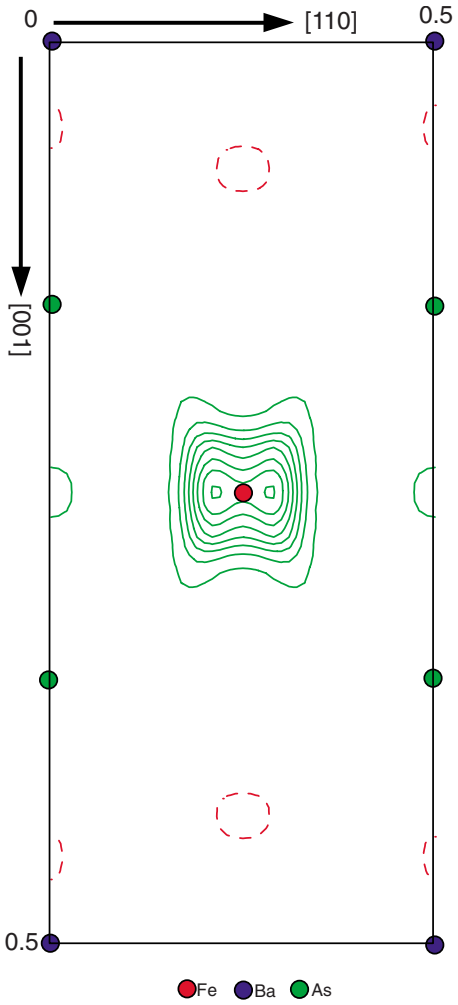

FIG. 2. (Color online) Maximum-entropy reconstruction of the magnetization distribution in tetragonal $BaFe_2As_2$ at 200 K projected down $[1\bar{1}0]$. Contours are drawn at intervals of 10^{-2} $\mu_B Å^{-2}$.

The method of maximum entropy[29,30] provides a model free method for reconstructing an image from sparse and noisy data. We have used this method to clarify the shape of the distribution. The maximization procedure coded in the MEMSYS III subroutine library[31] was used to make the maximum entropy reconstruction of the magnetization distribution projected down $[1\bar{1}0]$, from the measured magnetic structure factors. The result of the reconstruction is shown in Fig. 2. The reconstruction shows clearly that the magnetization is confined to the region around the iron atoms and that there is no significant magnetization associated with either As or Ba atoms. The magnetization around the Fe atom is significantly nonspherical with a shape that appears to extend in the [111] directions of the projection. Further clarification of the shape of the iron-atom magnetization was obtained by fitting the magnetic structure factors to a multipole model in which they are expressed as

TABLE III. Fe Multipole amplitudes and 3*d* orbital occupancies determined from the magnetic structure factors determined for $BaFe_2As_2$ at 200 K.

		Amplitudes ($m\mu_B$)	
Function	Coeff.	All *d* [a]	t_{2g} only[b]
$Y(00)$	a_0	6.3(2)	6.4(2)
$Y(20)$	a_{20}	−1.6(9)	−1.15(6)
$Y(40)$	a_{40}	−2(3)	−1.3(4)
$Y(44+)$	a_{44}	−8(4)	−2.8(5)
χ^2		0.87	0.88
		Occupancies (%)	
Orbital	All *d* [a]	t_{2g} only[b]	
$3z^2-r^2$	−16(28)	0	
x^2-y^2	−42(36)	0	
xy	98(36)	52(6)	
xz, yz	61(6)	48(6)	

[a]All multipole parameters allowed by $\bar{4}m2$ point symmetry.
[b]Multipole parameters constrained to give only t_{2g}-type orbitals.

$$F_M(\mathbf{k}) = a_0\langle j_0(|\mathbf{k}|)\rangle + \sum_{l=2,4}\langle j_l(|\mathbf{k}|)\rangle \sum_{m=-l}^{m=l} a_{lm} Y_{\hat{\mathbf{k}}}(lm\pm),$$

where the $\langle j_l(|\mathbf{k}|)\rangle$ are the form factor integrals for a neutral Fe atom[28] and the $Y_{\hat{\mathbf{k}}}(lm\pm)$ are the real combinations of spherical harmonic functions

$$Y_{\hat{\mathbf{k}}}(lm\pm) = \frac{1}{\sqrt{2}}[Y_l^{-m}(\hat{\mathbf{k}}) \pm (-1)^m Y_l^m(\hat{\mathbf{k}})].$$

The point-group symmetry of the Fe site, $\bar{4}m2$, limits the nonzero coefficients a_{lm} to a_{20}, a_{40}, and a_{44}, and the values of the four coefficients obtained from the least-squares fit are given in Table III.

In a site with fourfold symmetry the *d*-electron orbitals split into three singlet states: $d_{3z^2-r^2}$, $d_{x^2-y^2}$, and d_{xy} and a doublet combination of d_{xz} and d_{yz}. The first two singlet states are derived from the cubic e_g functions and the third singlet and the doublet from the t_{2g} ones. The occupancies of these four nondegenerate orbitals can be derived directly from the coefficients a_{lm}. However the parameters obtained from the unconstrained fit lead to unphysical, negative occupancies for the two e_g-type orbitals but with large estimated standard deviations. A constrained fit in which the ratio between the a_{lm} was fixed to correspond to occupancy of the t_{2g}-type orbitals only, gave equally good agreement as shown in Table III. The magnetic structure factors calculated for this constrained multipole model and also those obtained for the best spherically symmetric model are given together with the measured values and the diamagnetic corrections in Table II.

The magnetic form factor of Fe in the antiferromagnetic phase of the closely related pnictide superconductor $SrFe_2As_2$ has been studied in two recent investigations.[32,33] Whereas one of the publications[32] concludes that the magnetization distribution is significantly extended in the directions of the FeAs bonds, the density-functional theory (DFT) calculations made in the other,[33] which also predicts significant anisotropy in the magnetization distribution around the Fe atom, suggests that the most significant extension is rather in ⟨100⟩ and ⟨110⟩ directions. The apparently large anisotropy reported by Ratcliff *et al.*[32] was deduced from Fourier inversion of the antiferromagnetic form factor. It is probably largely an artifact introduced because the experiment only measures the Fourier components of magnetization in the plane perpendicular to the magnetization direction and hence the Fourier inversion lacks components which would modulate the density in directions perpendicular to the spin. The apparent extension is accentuated by the intervention of nodal planes characterizing the antiferromagnetic arrangement. The paramagnetic magnetization distribution measured in the present experiment is projected on the plane perpendicular to the magnetization direction so that Fourier components with all orientations in the plane of projection can be measured. It has the same periodicity as the crystal lattice and so cannot be compared directly with an antiferromagnetic magnetization distribution which has systematic nodes imposed by the antiferromagnetic structure.

The polarized neutron technique has been widely used to determine the distribution of electrons giving rise to the paramagnetism in many systems. The classical work on paramagnetic metals is reviewed by Moon,[34] and its application to cuprate superconductors by Boucherle *et al.*[35] In all cases the paramagnetic magnetization arises from redistribution, by the magnetizing field, of electrons of opposite spin in states near the Fermi surface and the magnitude of their contribution is proportional to their density of states at the Fermi surface. These electrons will only be the same as those giving rise to the antiferromagnetic moment if that moment is due to unpaired states in narrow bands just below the Fermi surface.

The results of the present experiment show that at least 96% of the electrons in $BaFe_2As_2$, which give rise to the paramagnetic susceptibility, are localized on the Fe atoms with a radial distribution similar to that of a neutral Fe atom. Their angular distribution shows that they occupy the t_{2g}-type orbitals with a strong preference for the singly degenerate *xy* type which has its maxima in the ⟨110⟩ directions which are not those of any ligand atoms rather than the doubly degenerate *xz* and *yz* types which maximize in a cone containing directions nearly parallel to the Fe-As bond directions. This anisotropy is broadly in agreement with the results of the DFT calculations[33] for antiferromagnetic $SrFe_2As_2$. If, as might be expected, there is strong hybidization between Fe and As atoms these hybridized bonding and antibonding states must lie well below and well above the Fermi level leaving narrow 3*d* nonbonding bands at the Fermi surface.

[1] Y. Kamihara, T. Watanabe, M. Hirano, and H. Hosono, J. Am. Chem. Soc. **130**, 3296 (2008).
[2] H. Takahashi, K. Igawa, K. Arii, Y. Kamihara, M. Hirano, and H. Hosono, Nature (London) **453**, 376 (2008).
[3] X. H. Chen, T. Wu, G. Wu, R. H. Liu, H. Chen, and D. F. Fang, Nature (London) **453**, 761 (2008).
[4] S. Matsuishi, Y. Inoue, T. Nomura, H. Yanagi, M. Hirano, and H. Hosono, J. Am. Chem. Soc. **130**, 14428 (2008).
[5] M. Rotter, M. Tegel, and D. Johrendt, Phys. Rev. Lett. **101**, 107006 (2008).
[6] H. H. Wen, G. Mu, L. Fang, H. Yang, and X. Zhu, EPL **82**, 17009 (2008).
[7] Z.-A. Ren, W. Lu, J. Yang, W. Yi, X.-L. Shen, Zheng-Cai, G.-C. Che, X.-L. Dong, L.-L. Sun, F. Zhou, and Z.-X. Zhao, Chin. Phys. Lett. **25**, 2215 (2008).
[8] S. Matsuishi, Y. Inoue, T. Nomura, M. Hirano, and H. Hosono, J. Phys. Soc. Jpn. **77**, 113709 (2008).
[9] P. Cheng, B. Shen, G. Mu, X. Zhu, F. Han, B. Zeng, and H. Wen, EPL **85**, 67003 (2009).
[10] M. S. Torikachvili, S. L. Bud'ko, N. Ni, P. C. Canfield, Phys. Rev. Lett. **101**, 057006 (2008).
[11] P. L. Alireza, Y. T. C. Ko, J. Gillett, C. M. Petrone, J. M. Cole, G. G. Lonzarich, and S. E. Sebastian, J. Phys.: Condens. Matter **21**, 012208 (2009).
[12] C. de la Cruz, Q. Huang, J. W. Lynn, J. Li, W. Ratcliff II, J. L. Zarestky, H. A. Mook, G. F. Chen, J. L. Luo, N. L. Wang, and P. C. Dai, Nature (London) **453**, 899 (2008).
[13] Q. Huang, Y. Qiu, W. Bao, M. A. Green, J. W. Lynn, Y. C. Gasparovic, T. Wu, G. Wu, and X. H. Chen, Phys. Rev. Lett. **101**, 257003 (2008).
[14] Y. Su, P. Link, A. Schneidewind, T. Wolf, P. Adelmann, Y. Xiao, M. Meven, R. Mittal, M. Rotter, D. Johrendt, T. Brueckel, and M. Loewenhaupt, Phys. Rev. B **79**, 064504 (2009).
[15] A. I. Goldman, D. N. Argyriou, B. Ouladdiaf, T. Chatterji, A. Kreyssig, S. Nandi, N. Ni, S. L. Bud'ko, P. C. Canfield, and R. J. McQueeney, Phys. Rev. B **78**, 100506(R) (2008).
[16] Y. Xiao, Y. Su, R. Mittal, T. Chatterji, T. Hansen, C. M. N. Kumar, S. Matsuishi, H. Hosono, and Th. Brueckel, Phys. Rev. B **79**, 060504(R) (2009).
[17] C. C. Lee, W. G. Yin, and W. Ku, Phys. Rev. Lett. **103**, 267001 (2009).
[18] J. Zhao, Q. Huang, C. de la Cruz, S. Li, J. W. Lynn, Y. Chen, M. A. Green, G. F. Chen, G. Li, Z. Li, J. L. Luo, N. L. Wang, and P. Dai, Nature Mater. **7**, 953 (2008).
[19] J. G. Bednorz and K. A. Mueller, Z. Phys. B: Condens. Matter **64**, 189 (1986).
[20] R. Mittal, Y. Su, S. Rols, T. Chatterji, S. L. Chaplot, H. Schober, M. Rotter, D. Johrendt, and Th. Brueckel, Phys. Rev. B **78**, 104514 (2008).
[21] R. Mittal, Y. Su, S. Rols, M. Tegel, S. L. Chaplot, H. Schober, T. Chatterji, D. Johrendt, and Th. Brueckel, Phys. Rev. B **78**, 224518 (2008).
[22] A. D. Christianson, E. A. Goremychkin, R. Osborn, S. Rosenkranz, M. D. Lumsden, C. D. Malliakas, I. S. Todorov, H. Claus, D. Y. Chung, M. G. Kanatzidis, R. I. Bewley, and T. Guidi, Nature (London) **456**, 930 (2008).
[23] M. D. Lumsden, A. D. Christianson, D. Parshall, M. B. Stone, S. E. Nagler, G. J. MacDougall, H. A. Mook, K. Lokshin, T. Egami, D. L. Abernathy, E. A. Goremychkin, R. Osborn, M. A. McGuire, A. S. Sefat, R. Jin, B. C. Sales, and D. Mandrus, Phys. Rev. Lett. **102**, 107005 (2009).
[24] S. Chi, A. Schneidewind, J. Zhao, L. W. Harriger, L. Li, Y. Luo, G. Cao, X. Zhu'an, M. Loewenhaupt, J. Hu, and P. Dai, Phys. Rev. Lett. **102**, 107006 (2009).
[25] C. Stassis, Phys. Rev. Lett. **24**, 1415 (1970).
[26] R. Maglic, T. O. Brun, G. P. Felcher, Y. K. Chang, and J. B. Ketterson, J. Magn. Magn. Mater. **9**, 318 (1978).
[27] E. N. Maslen, A. G. Fox, and M. A. O'Keefe, in *International Tables for Crystallography*, (Kluwer, Dordrecht, 1992), Table 6.1.1.4, p. 500.
[28] A. J. Freeman and R. E. Watson, Acta Crystallogr. **14**, 231 (1961).
[29] *Maximum Entropy and Bayesian Methods*, edited by J. Skilling (Kluwer, Dordrecht, 1989).
[30] R. J. Papoular and B. Gillon, Europhys. Lett. **13**, 429 (1990).
[31] S. F. Gull and J. Skilling, MEMSYS III Quantified Maximum Entropy Subroutine Library, Meldreth, U.K., 1989.
[32] W. Ratcliff II, P. A. Kienzle, J. W. Lynn, S. Li, P. Dai, G. F. Chen, and N. L. Wang, Phys. Rev. B **81**, 140502(R) (2010).
[33] Y. Lee, D. Vaknin, H. Li, W. Tian, J. L. Zarestky, N. Ni, S. L. Budko, P. C. Canfield, R. J. McQueeney, and B. N. Harmon, Phys. Rev. B **81**, 060406(R) (2010).
[34] R. M. Moon, Physica B **137**, 19 (1986).
[35] J.-X. Boucherle, J. Y. Henry, R. J. Papoulr, J. Rossat-Mignod, J. Schweizer, F. Tasset, and G. Uimin, Physica B **192**, 25 (1993).